Magnetic susceptibility of $NdGaO_3$ at low temperatures: A quasi-two-dimensional Ising behavior

F. Luis, M. D. Kuz'min, F. Bartolomé, V. M. Orera, and J. Bartolomé
Instituto de Ciencia de Materiales de Aragón, CSIC-Universidad de Zaragoza, Plaza San Francisco S/N, 50009 Zaragoza, Spain

M. Artigas and J. Rubín
Departamento Ciencia y Tecnología de Materiales y Fluidos, CPS and I.C.M.A., 50015 Zaragoza, Spain
(Received 3 February 1998)

The ac magnetic susceptibility of a $NdGaO_3$ single crystal has been measured along the three principal crystallographic axes in the temperature range from 50 K down to 0.07 K. The data obtained indicate that the compound orders antiferromagnetically at $T_N \approx 1$ K with the sublattice moments parallel to [001], which is consistent with earlier neutron-diffraction results. The data are interpreted in terms of the Ising model on the simple tetragonal lattice in the quasi-two-dimensional regime: the intralayer exchange is relatively strong and antiferromagnetic, $J_\perp/k = -0.70$ K, whereas the interlayer exchange is ferromagnetic and an order of magnitude weaker, $J_\parallel/k = 0.07$ K. This model also describes well the earlier specific-heat data. The g factors deduced from the low-temperature susceptibility, $g_x = 1.84$, $g_y = 2.41$, $g_z = 2.73$, are in reasonable agreement with electron paramagnetic resonance measurements on Nd-doped $LaGaO_3$. [S0163-1829(98)02625-3]

I. INTRODUCTION

Rare-earth oxide compounds with perovskite structure have a long record of outstanding performance in solid-state physics. In the last decade they received a renewed attention in connection with the discovery of high-T_C superconductivity and, more recently, giant magnetoresistance. Many perovskite materials have been thoroughly studied and are now used in industry.

Neodymium gallate, $NdGaO_3$ is one such compound. It is commonly used as a substrate for high-temperature superconductor thin-film deposition because of a good lattice and thermal expansion match, in particular with YBaCuO.[1] This is due to the fact that, like many other important perovskites, $NdGaO_3$ has an orthorhombically distorted structure [space group D_{2h}^{16}-$Pbnm$, (Ref. 2)], and at the same time it is a paradigm of passive stability. On account of such use, large single crystals of $NdGaO_3$ are now available commercially.

This image of something inert and plain changed when a sharp λ anomaly was discovered in the specific heat of $NdGaO_3$ at $T_N = 0.97 \pm 0.01$ K.[3] That anomaly was then ascribed to an antiferromagnetic ordering of the Nd moments and it was found that the XY model on the simple cubic lattice gave an accurate account of the observed low-temperature specific heat.

However, a subsequent neutron-diffraction study[4] suggested a C_z configuration of the ordered Nd moments (notation of Bertaut[5]) as well as a fairly isotropic g factor. Realization of the spin configuration C_z implied a coexistence of ferromagnetic and antiferromagnetic exchange interactions between different types of nearest neighbors, impossible in the simple cubic lattice. The nearly isotropic g factor was hard to reconcile with the XY model.

To verify those findings and to resolve the apparent contradiction, we undertook a study of the initial magnetic susceptibility of $NdGaO_3$ at low temperatures. The only earlier susceptibility study[6] had been limited to temperatures above 4.2 K and had failed to unambiguously refer the data, therein called $\chi_\parallel$ and $\chi_\perp$, to crystallographic directions.

Presented below is our study of the ac susceptibility of $NdGaO_3$ along the three orthorhombic axes at temperatures down to 0.07 K. It also includes a model that describes consistently the susceptibility data as well as the earlier specific-heat data[3] and the neutron-diffraction data[4] in terms of the Ising model on the anisotropic tetragonal lattice.

II. EXPERIMENTAL DETAILS

The $NdGaO_3$ single crystal, grown by the Bridgman technique, was cut as a parallelepiped with the edges parallel to [100], [010], and [001]. The ac susceptibility below 3.5 K was measured with a mutual inductance coil wound on a glass tube placed under the mixing chamber of a ^{3}He-^{4}He dilution refrigerator. The sample was oriented and glued onto a plastic sample holder located in the center of one of two oppositely wound secondary coils. The excitation amplitude was 1 mOe and the frequency $f = 160$ Hz. The signal was measured by means of a low-impedance ac bridge in which a superconducting quantum interference device (SQUID) (SHE Corporation model MFP/MFPC) was employed as null detector.[7] Above 1.8 K the measurements were performed on a Quantum Design SQUID magnetometer MPMS5 using the ac susceptibility mode. The data in the overlap region between 1.8 and 3.5 K were used to convert the low-temperature data from arbitrary into absolute units. The absolute accuracy of the data was 5%, while the relative error was better than 1%.

X-band electron paramagnetic resonance (EPR) measurements were performed on Nd:$LaGaO_3$ as well as pure $NdGaO_3$ powder samples (prepared by hand crushing small amounts of the original single crystals) at temperatures from 4.2 to 77 K using a Brucker ESP-380E spectrometer. The diphenylpicrylhydrazyl signal ($g = 2.0037 \pm 0.0002$) was

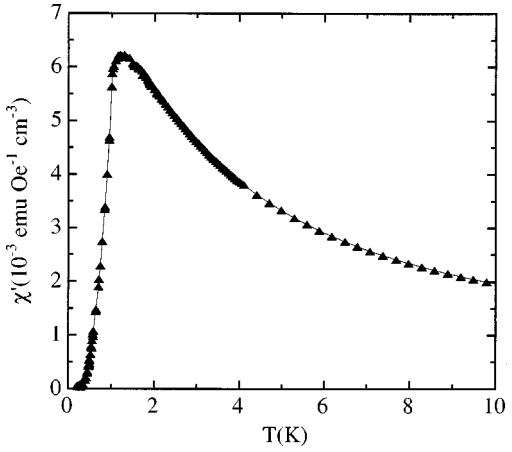

FIG. 1. Magnetic susceptibility of $NdGaO_3$ along [001].

used to measure the microwave frequency. The Nd content of the doped $LaGaO_3$ sample was determined by electron probe microanalysis to be $(2.1\pm0.3)\times10^{20}$ Nd^{3+} ions/cm^3.

III. EXPERIMENTAL RESULTS

A. Magnetic susceptibility

The magnetic susceptibility of $NdGaO_3$ along the c axis χ_z, is shown in Fig. 1. It increases as temperature decreases down to 1.1 K, where it has a rounded maximum. Below this temperature it shows a steep decrease with an inflexion point at $T_N=1.00\pm0.05$ K which is, within the experimental error, in good agreement with the magnetic ordering transition temperature determined from the heat capacity measurements, $T_N=0.97\pm0.01$ K. The decrease in χ_z below T_N is characteristic of the susceptibility $\chi_{\|}$ along the sublattices of a collinear antiferromagnet. Indeed, as $T\rightarrow0$, χ_z tends to zero, within the experimental error.

The susceptibilities in the a and b directions, χ_x and χ_y, are alike (see Fig. 2, curves a and b, respectively). Both χ_x and χ_y increase as the temperature decreases down to 1.1 K, where both have rounded maxima. Below this temperature they slightly decrease, the respective inflexion points being both situated at 1.0 ± 0.01 K, in good agreement with the T_N determined above, and tend to nonzero constant values as T decreases down to 0.07 K. In spite of the similarity, χ_y is 30% larger than χ_x. Such behavior is characteristic of the transverse susceptibility $\chi_{\perp}$ of an antiferromagnet, with different g factors along the a and b axes.

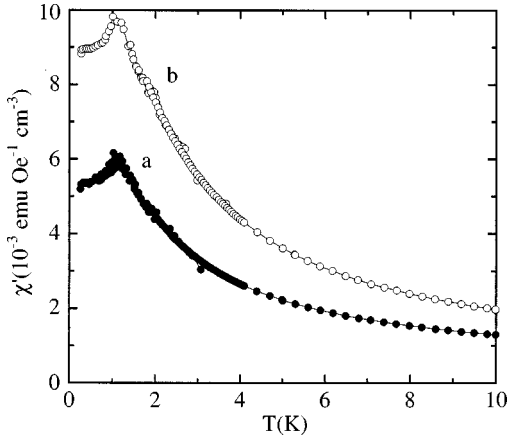

FIG. 2. Magnetic susceptibility of $NdGaO_3$ along [100] (a), and [010] (b).

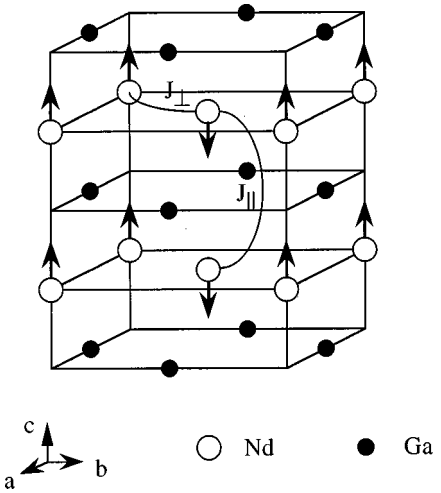

FIG. 3. Magnetic structure C_z of $NdGaO_3$ (oxygen atoms are not depicted).

These results corroborate the C_z magnetic structure below T_N, proposed after the neutron-diffraction experiments.[4] This structure, represented schematically in Fig. 3, can be described as antiferromagnetically ordered layers of Nd moments, coupled ferromagnetically to the adjacent layers, the sublattices being parallel to the c axis. We shall take $T_N=0.97\pm0.01$ K, determined from heat capacity data, for the Néel point, since this value has higher accuracy than that determined from the present susceptibility measurements. Below, we shall regard this T_N value as a fixed parameter in our interpretation of the susceptibility data.

B. EPR spectrometry

The EPR signal could only be detected in Nd-doped $LaGaO_3$ below 20 K, while no signal was observed in the pure $NdGaO_3$ samples, presumably because of the strong line broadening caused by the magnetic interaction between the Nd^{3+} ions. Figure 4 shows the powder spectrum of the Nd-doped $LaGaO_3$ sample measured at $T=11$ K. The lowest $^4I_{9/2}$ multiplet of the Nd^{3+} ion is split into five Kramers doublets by crystal-field effects. The ground state is a dou-

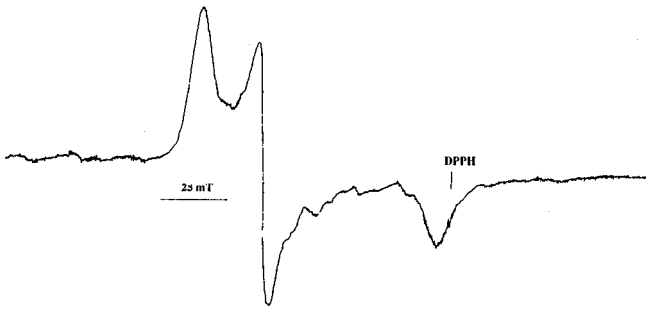

FIG. 4. EPR spectrum of a powder sample of $LaGaO_3$ doped with 1% of Nd.

blet, with the next excited state lying at 11.4 meV=132 K.[6] Thus, as expected, the pattern is typical of an ion with a doublet ground state, and the principal g values are $g_1 = 2.72 \pm 0.01$, $g_2 = 2.495 \pm 0.001$, and $g_3 = 2.025 \pm 0.005$.

Some small-intensity satellites (whose intensity is less than 2% of that of the central lines) can be observed on the low- and high-field sides of the main signal. Their relative intensities and magnetic-field shifts are typical of hyperfine structures due to the isotopes ^{143}Nd ($I = \frac{7}{2}$, natural abundance 12.2%) and ^{145}Nd ($I = \frac{7}{2}$, natural abundance 8.3%). Unfortunately, the low signal-to-noise ratio and the complexity of the spectrum prevented us from determining the hyperfine interaction parameters.

IV. ANALYSIS AND DISCUSSION

Despite its original success in describing the low-temperature specific heat, the simple cubic XY model had to be abandoned in the face of the later neutron-diffraction data,[4] which revealed that the magnetic structure of Nd in the ordered phase is C_z. Such spin configuration (see Fig. 3) suggests that, unlike in the simple cubic lattice, where all six nearest neighbors are equivalent, the exchange interaction in $NdGaO_3$ is strongly direction dependent, being ferromagnetic between the neighbors ''above'' and ''below'' and antiferromagnetic between those in the same basal plane. This might have been expected, since the low crystallographic symmetry, with just a horizontal mirror plane through the Nd sites, can only guarantee the equivalence of the two nearest Nd neighbors above and below the central Nd ion, whereas the four neighbors in the basal plane are all different from each other and from the former two.

For simplicity, however, in this work the Nd ions were assumed to occupy the nodes of a simple tetragonal lattice, with just two types of neighborships—along the c axis ($\parallel$) and in the basal plane ($\perp$). Accordingly, our starting point was a bilinear exchange Hamiltonian of general form, compatible with the tetragonal symmetry and limited, as is usual for oxide compounds, to the nearest neighbors:

$$\hat{H}_{\rm ex} = -2J_{\parallel} \sum_{\substack{i>j \\ \parallel {\rm NN}}} \hat{S}_i^z \hat{S}_j^z - 2J'_{\parallel} \sum_{\substack{i>j \\ \parallel {\rm NN}}} (\hat{S}_i^x \hat{S}_j^x + \hat{S}_i^y \hat{S}_j^y) - 2J_{\perp} \sum_{\substack{i>j \\ \perp {\rm NN}}} \hat{S}_i^z \hat{S}_j^z - 2J'_{\perp} \sum_{\substack{i>j \\ \perp {\rm NN}}} (\hat{S}_i^x \hat{S}_j^x + \hat{S}_i^y \hat{S}_j^y). \quad (1)$$

Here the symbol $\parallel$NN ($\perp$NN) means that the corresponding sum is taken over such nodes i and j, which are nearest neighbors linked by a segment parallel (perpendicular) to the c axis. $\hat{S}_i^{\alpha}$, $\alpha = x,y,z$, are the effective spin ($S = \frac{1}{2}$) operators for the ith lattice node. Our approach was thus limited to temperatures below ~ 50 K, where only the ground Kramers doublet of Nd^{3+} is appreciably populated.

For calculating magnetic susceptibility, terms describing the interaction with applied magnetic field had to be included in the Hamiltonian, which then took the following form:

$$\hat{H} = \hat{H}_{\rm ex} + \mu_B \sum_i (H_x g_x \hat{S}_i^x + H_y g_y \hat{S}_i^y + H_z g_z \hat{S}_i^z) - \tfrac{1}{2}(\chi_x^{\rm VV} H_x^2 + \chi_y^{\rm VV} H_y^2 + \chi_z^{\rm VV} H_z^2). \quad (2)$$

Here the first term, $\hat{H}_{\rm ex}$ of Eq. (1), stands for the Nd-Nd exchange; the second term is the standard anisotropic Zeeman operator, g_{α} are the g factors of the ground Kramers doublet of Nd^{3+}; the third term describes the Van Vleck susceptibility due to field-induced admixing of the excited doublets to the ground doublet. The inclusion of the Van Vleck term is motivated by its essential role in explaining the magnetic properties of the related compounds $NdFeO_3$ (Ref. 8) and $DyFeO_3$.[9] The last two terms in Eq. (2) comply with orthorhombic rather than tetragonal symmetry, which allows $g_x \neq g_y$ and $\chi_x^{\rm VV} \neq \chi_y^{\rm VV}$. The apparent inconsistency is due to our search for a model with as few adjustable parameters as would prove sufficient for an adequate description of the experimental data (thus, though the monoclinic local symmetry of the Nd site admits a nondiagonal g-tensor component g_{xy}, it was neglected).

The temperature range under study naturally splits into three subranges: 5–50 K, 1–5 K, and 0.07–1 K, which we found advantageous to analyze sequentially, starting with the highest temperature one.

A. Temperature range 5–50 K

As $T \gg T_N$, the high-temperature approximation was applied to the partition function obtained from the solution of the Hamiltonians (1) and (2), which lead to the following expressions for the molar specific heat and volume susceptibility:[10]

$$C_p/R = aT^{-2}, \quad (3)$$

$$\chi_{\alpha} = \frac{c_{\alpha}}{T - \theta_{\alpha}} + \chi_{\alpha}^{\rm VV}, \quad \alpha = x,y,z, \quad (4)$$

where

$$a = \frac{1}{4}\left(\frac{J_{\parallel}}{k}\right)^2 + \frac{1}{2}\left(\frac{J'_{\parallel}}{k}\right)^2 + \frac{1}{2}\left(\frac{J_{\perp}}{k}\right)^2 + \left(\frac{J'_{\perp}}{k}\right)^2, \quad (5)$$

$$c_{\alpha} = N\mu_B^2 g_{\alpha}^2/4k, \quad (6)$$

$$\theta_x = \theta_y = \frac{J'_{\parallel}}{k} + 2\frac{J'_{\perp}}{k}, \quad (7)$$

$$\theta_z = \frac{J_{\parallel}}{k} + 2\frac{J_{\perp}}{k}. \quad (8)$$

Here, $N = 1.73 \times 10^{22}$ cm^{-3} is the concentration of the Nd ions.

Expressions (3)–(8) were then used to fit the experimental data between 5 and 50 K. From the fit to the high-temperature tail of the heat capacity, the value $a = 0.35 \pm 0.02$ K^2 was obtained. The susceptibility data were fitted satisfactorily with Eq. (4) (see Fig. 5). The values of adjustable parameters are collected in Table I.

The fits already demonstrate the anisotropic character of the system, with a g factor that is highest along the c axis, and lowest along the a axis. The fact that $\theta_x \approx \theta_y$ provides some support for the use of the tetragonal approximation in the exchange Hamiltonian (1). The value of the Van Vleck

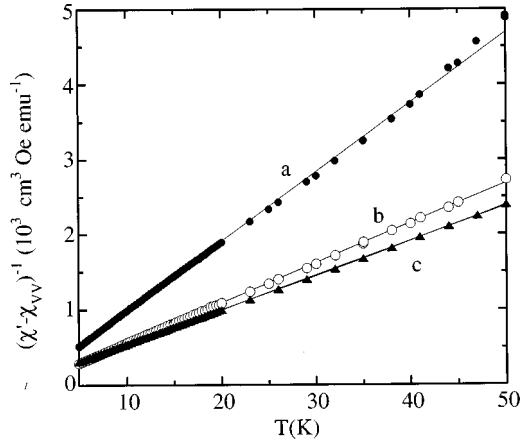

FIG. 5. Inverse susceptibility (after subtraction of the Van Vleck term) vs temperature along the three principal crystallographic axes a, b, and c. The lines were calculated with Eq. (4) and the parameters listed in Table I.

susceptibility along [100], $\chi_x^{VV}=2.9\times10^{-4}$ emu Oe^{-1} cm^{-3}, is comparable to the value $\chi_x^{VV}=4.2\times10^{-4}$ emu Oe^{-1} cm^{-3} deduced from neutron-diffraction experiments in $NdFeO_3$, and justifies ''*a posteriori*'' the inclusion of the Van Vleck term in Eq. (2).[8]

It was found convenient to use the coordinate plane $J_\perp$-$J_\parallel$, Fig. 6, for the analysis of possible values of the exchange parameters. The observed spin configuration C_z, Fig. 3, implies that z components of the Nd spins interact ferromagnetically if the exchange link is parallel to the c axis and antiferromagnetically if it is in the basal plane, i.e., that $J_\parallel>0$ and $J_\perp<0$. For this reason the analysis was restricted to the second quadrant of the $J_\perp$-$J_\parallel$ plane. Moreover, by virtue of Eq. (8), with $\theta_z=-1.8\pm0.3$ K as found from the susceptibility data, the values of $(J_\perp, J_\parallel)$ must be confined to the hatched area of Fig. 6.

Assuming at first zero values for $J'_\parallel$ and $J'_\perp$, we further found from Eq. (5) with $a=0.35\pm0.02$ K^2 that the solution had at the same time to be situated within the narrow zone delimited by two ellipses centered at the origin (part of this zone within the second quadrant is hatched horizontally in Fig. 6), the intersection of this zone and the hatched stripe must contain the solution sought. The previous assumption is now justified; since any significantly nonzero $J'_\parallel$ or $J'_\perp$ would lead to a contraction of the elliptic ring and disappearance of the intersection area. We thus conclude that $J'_\parallel$ and $J'_\perp$ must be small (and most likely negative), $J'_\parallel\approx J'_\perp\approx-0.1$ K, just enough to satisfy Eq. (7) without forcing the intersection area of Fig. 6 into nonexistence. $J_\parallel$, too, appears to be small, but positive, $J_\parallel/k\sim0.1$ K. Finally, $J_\perp$ is the dominant exchange parameter, $J_\perp/k\approx-0.8$ K.

TABLE I. g factor, Weiss constant, and van Vleck susceptibility obtained from the fits of Eq. (4).

Axis	g_α	θ_α (K)	$\chi_\alpha^{VV}\times10^4$ emu Oe^{-1} cm^{-3}
x	1.98 ± 0.01	-0.6 ± 0.4	2.9 ± 0.1
y	2.63 ± 0.01	-0.5 ± 0.3	1.9 ± 0.1
z	2.83 ± 0.01	-1.8 ± 0.3	1.3 ± 0.1

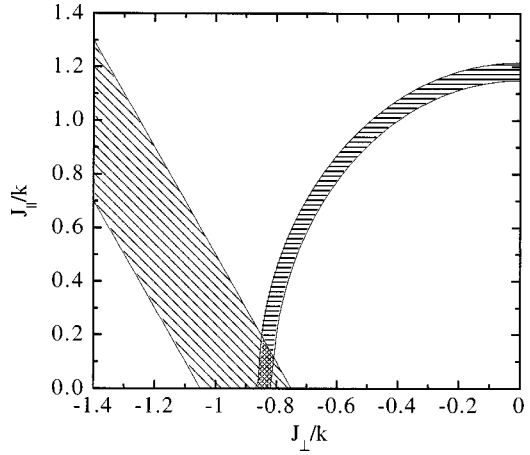

FIG. 6. Graphical analysis of possible values of $J_\parallel$ and $J_\perp$.

B. Temperature range 1–5 K

This range, which includes the Néel point, required a more elaborate treatment. To make that possible, we set the small parameters $J'_\parallel$ and $J'_\perp$ to zero and thus arrived at the Ising model on a simple tetragonal lattice, with two types of neighborships:

$$\hat{H}_{ex}=-2J_\parallel\sum_{\substack{i>j\\ \parallel NN}}\hat{S}_i^z\hat{S}_j^z-2J_\perp\sum_{\substack{i>j\\ \perp NN}}\hat{S}_i^z\hat{S}_j^z. \tag{9}$$

The Van Vleck term in Eq. (2) was omitted as the temperature-independent Van Vleck susceptibility becomes relatively less important at low temperatures. In short, we have reduced the problem to a simple Ising model with antiferromagnetic layers weakly coupled ferromagnetically.

The statistics of the model described by Eq. (9) is governed by the ratio $r=J_\parallel/J_\perp$ between the interlayer and intralayer exchange integrals, $r=0$ being an important particular case, when the system splits into two-dimensional simple quadratic (s.q.) lattices. Our own case $r\approx-0.1$, seems to fall into the region of crossover from the three-dimensional (3D) to 2D regime.

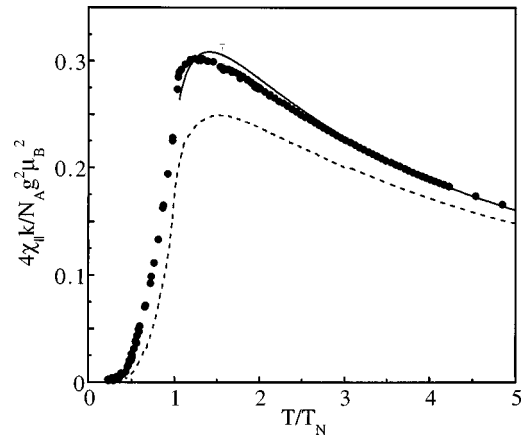

FIG. 7. Scaled experimental susceptibility along [001] (after subtraction of χ_z^{VV}) ($g_z=2.73$, $J_\perp=-0.70$ K and $T_N=0.97$ K), compared with calculated curves for the parallel susceptibility. (—) $r=-0.1$, from high-temperature series, Eq. (10). (--) for $r=0$, from Ref. 13.

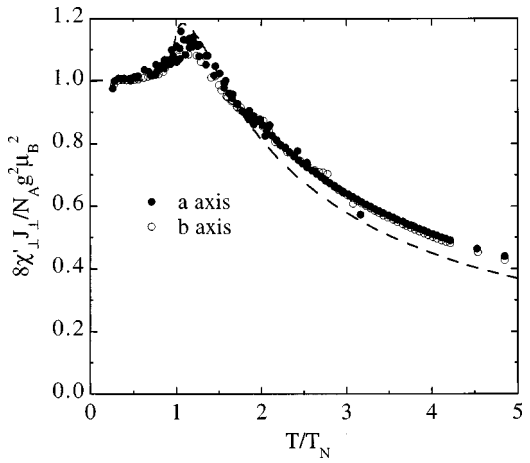

FIG. 8. Scaled experimental susceptibility along [100] (after subtraction of χ_x^{VV}) ($g_x=1.80$), and [010] (after subtraction of χ_x^{VV}) ($g_y=2.28$) with $J_\perp=-0.86$ K and $T_N=0.97$ K. (--) $r=0$, theoretical curve for the perpendicular susceptibility, from Ref. 14.

The critical properties in the 2D-3D crossover with $J_\perp>0$ had been analyzed[11] by Padé approximants (PA) methods. We have applied the same approximations and algorithms to analyze the $J_\perp<0$ case of our interest. For an arbitrary value of $J_\perp$ and r the reduced susceptibility has been calculated with the expression

$$\overline{\chi}(J_\perp,r)=\frac{4kT\chi_\parallel}{Ng_z^2\mu_B^2}=\overline{\chi}_2+\frac{rJ_\perp}{kT}\overline{\chi}_2^2+\mathrm{PA}\left[\overline{\chi}-\left(\overline{\chi}_2+\frac{rJ_\perp}{kT}\overline{\chi}_2^2\right)\right], \tag{10}$$

where $\overline{\chi}$ corresponds to the high-temperature series of the reduced susceptibility for arbitrary $J_\perp$ and r,[12] and $\overline{\chi}_2$ is the square planar Ising $S=\frac{1}{2}$ parallel reduced susceptibility.[13]

We tried several r values close to $-\frac{1}{8}$ (obtained from the previous section) and found that the height and position of the maximum was not particularly sensitive to small variations of r (the same had been previously observed in Navarro and de Jongh, 1978).[11] The theoretical curves of the scaled susceptibility for $r=0$ and $r=-0.1$ are given in Fig. 7. A good agreement with the experimental data (corrected for the Van Vleck contribution) was achieved for $r=-0.1$, for which $kT_c/J_\perp=1.3807$, then substituting $T_c=T_N$ we find $J_\perp=-0.70\pm0.01$ K. This agrees well with the estimation $J_\perp/k\approx-0.8$ K from the previous section. For better overall agreement, we finally had to scale the data slightly in the vertical scale in Fig. 7, by $g_z=2.73$, rather than 2.83, as found in Sec. IV A (see Table II). The difference could be accounted for by the experimental error.

No theoretical predictions were available for the susceptibility perpendicular to the Ising axis at arbitrary r. We used the expression derived by Fisher[14] on the basis of Onsager's solution to the simple quadratic model[15] (dashed line in Fig. 8). This model predicts $kT_c/J_\perp=1.3846$, hence $J_\perp=-0.86\pm0.01$ K. For comparison, the experimental susceptibilities along the *a* and *b* axis were corrected for the Van Vleck contribution using the values of χ_x^{VV} and χ_y^{VV} previously deduced from the high-temperature data (Table I), $J_\perp=-0.86\pm0.01$ K and rescaling in the vertical scale to match the value at the susceptibility maximum, thus obtaining $g_x=1.80\pm0.02$ and $g_y=2.28\pm0.02$ that are close to the values deduced in the higher temperature region (see Table II).

This result can be checked with a reanalysis of our previous heat capacity data in terms of the same crossover Ising mode, assuming that the heat capacity critical behavior can be approximated by the expression, with $1/K_c=kT_c/J_\perp$ for the different r values as given in Ref. 11:

$$C/R=A\left(1-\frac{K}{K_c}\right)^{-\alpha}+e_0. \tag{11}$$

Since the crossover case $r=-0.1$ belongs topologically to the three-dimensional universality class, we have conjectured that the same singular behavior as for the simple cubic should be applicable; i.e., the exponent is identical ($\alpha=\frac{1}{8}$) while the amplitude A and constant e_0 are different.

To determine A for $r=-0.1$, we fixed the value $1/K_c=kT_C/J_\perp=1.3807$, and performed the Padé approximants analysis of the first derivative of the high-temperature heat capacity series, as given in Ref. 12.

$$A=\mathrm{PA}\left[\frac{\dfrac{dC/R}{dK}}{\dfrac{\alpha}{K_c}\left(1-\dfrac{K}{K_c}\right)^{-(\alpha+1)}}\right]. \tag{12}$$

The convergence was satisfactory, obtaining the amplitude $A=0.882\pm0.003$. The constant e_0 was obtained from the Padé approximants analysis of the difference series

$$e_0=\mathrm{PA}\left[C/R-A\left(1-\frac{K}{K_c}\right)^{-\alpha}\right], \tag{13}$$

which also converged satisfactorily yielding the value $e_0=-0.689\pm0.003$.

The heat capacity was calculated as

$$C/R=A\left(1-\frac{K}{K_c}\right)^{-\alpha}+e_0+\mathrm{PA}\left\{\sum_{n=2}^{\infty}(K/2)^n\left(\sum_{j=0}^{n}c_{nj}r^j\right)-\left[A\left(1-\frac{K}{K_c}\right)^{-\alpha}+e_0\right]\right\} \tag{14}$$

above $T_c=T_N$, as shown in Fig. 9. We observe an excellent agreement with the experimental data from T_N up to the highest temperatures measured. For comparison, we have plotted in the same figure the heat capacity for the $r=0$ case, as given by Onsager.

For the sake of completeness, we also calculated the critical entropy and energy above T_c making use of the heat capacity as written in Eq. (14). The results are included in Table III where they are compared with the experimental results. We note that the calculated critical entropy S_c/R is, within the experimental error, in agreement with the experimental value, while the calculated critical energy $-E_c/T_c$ is lower by 10%. The discrepancy in E_c can be attributed to an overestimation of the experimental high-temperature tail, which was extrapolated to $T\to\infty$ by means of a fitted T^{-2}

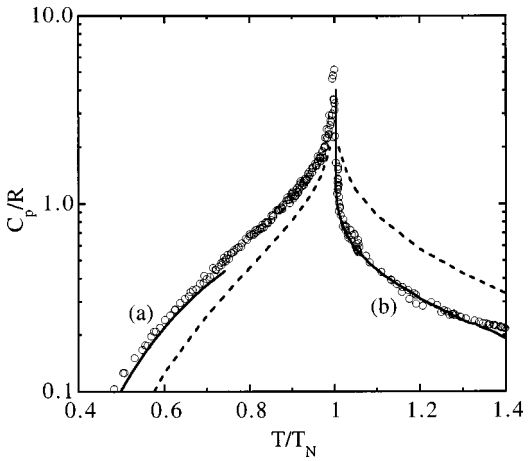

FIG. 9. Experimental heat capacity of $NdGaO_3$ vs reduced temperature ($T_N = 0.97$ K). (—) Calculated predictions for the 2D-3D crossover case with $|r| = 0.1$ from (a) spin-wave low-temperature series, (b) extrapolated high-temperature series. (--) Heat capacity for the antiferromagnetic simple quadratic $S = \frac{1}{2}$ model ($r = 0$).

law. In contrast, since the critical entropy is more sensitive to the temperature region near T_c, the error in the experimental determination is little affected by the high-temperature tail, and therefore the agreement is better.

C. Temperature range $0.07 < T < 1$ K

Below T_N there are no predictions of $\chi_\parallel$ for an arbitrary r value. However, there are numerical calculations for the square planar Ising case, $r = 0$.[13] We have drawn this theoretical curve scaled in reduced temperature T/T_N, with $kT_N/J_\perp = 1.1346$, together with our experimental data also scaled in temperature to T_N (Fig. 7). From inspection we conclude that the s.q. model ($r = 0$) describes almost quantitatively the low-temperature region below T_c, whereas it deviates more markedly as the temperature approaches $T_{\max}$. For temperatures higher than $T_{\max}$ the prediction for $r = 0$ is completely away from the data.

The perpendicular susceptibility for the $r = 0$ case[14] tends to the limit $\chi_\perp(T = 0) = Ng_\perp^2 \mu_B^2 / 8J_\perp$. Substituting the experimental data χ_x and χ_y at the lowest measured temperature for $\chi_\perp$ we obtain the values $g_x = 1.84$ and $g_y = 2.41$, practically identical to the values deduced from $\chi_{\perp,\max}$ (see Table II). In Fig. 8 we show the theoretical curve scaled to the $\chi_\perp(T = 0)$ value. We see that the temperature region extending up to $2T_c$ is quite well explained with the $r = 0$ model, though the curve diverges for higher temperatures.

The low-temperature tail of the heat capacity may be compared to the predictions for the low-temperature series developed for an arbitrary r.[16] We have plotted in Fig. 9 the resulting curve for $|r| = 0.1$, which mimics the experimental data for $T/T_C < 0.7$. By inspection of this figure we see that both the high- and low-temperature tails of the experimental anomaly are well accounted for by the theoretical predictions for the Ising crossover model with $|r| = 0.1$. For comparison, we have included in the same figure the prediction for the $r = 0$ model that differs radically from the predictions for $|r| = 0.1$. We conclude that the small interlayer interaction has a very strong effect on the shape and critical parameters of the heat capacity anomaly, far more than on the magnetic susceptibility.

V. CONCLUSIONS

The g_α fit parameters are collected in Table II, where they are compared with the g parameters deduced from the EPR data. They are somewhat different since, on one hand, the EPR data are obtained on a doped $Nd:LaGaO_3$ sample while the magnetic susceptibility is measured on a magnetically dense $NdGaO_3$ sample, although the electronic structure of the Nd^{3+} in both matrices is very similar.[17] On the other hand, the $g_{1.2.3}$ parameters are referred to the local g-tensor principal axes, which do not necessarily coincide with the crystallographic axes. However, it can be readily concluded that the highest value of g_1 can be assigned to the g_z, and since the other g_2 and g_3 parameters are not too different from the g_x and g_y fitted values, that the 2 and 3 axes are close to the a and b crystallographic axes, respectively.

The susceptibility and heat capacity data are explained by the same set of parameters within the $S = \frac{1}{2}$, Ising 2D to 3D crossover model. This result supports the restriction imposed by the neutron-diffraction data that the intralayer interaction should be negative while the interlayer interaction should be positive.

The quasi-two-dimensional characteristics of the magnetic properties of this material, which are caused by the small value of the interlayer interaction respect to the intralayer interaction, also suggests that small modifications in the interlayer exchange paths may give rise to changes of magnitude and even of sign of $J_\parallel$. Such sensibility of $J_\parallel$ to details in the interlayer interaction paths may explain that related perovskite compounds with essentially the same crystallographic structure and interatomic distances show very different magnetic structures. For example, the compounds $NdGaO_3$,[4] and $NdCoO_3$ (Ref. 18) order in the C_z configuration (which implies $J_\parallel < 0$) while $NdInO_3$ (Ref. 18) orders in

TABLE II. Critical temperature, g-tensor components, and exchange parameters obtained from the analysis of the experimental data.

Expt.	T_c (K)	g_x	g_y	g_z	$J_\perp/k$(K)	r
C_p	0.97 ± 0.01				-0.70 ± 0.01	-0.10 ± 0.02
$\chi_\parallel$				2.73 ± 0.02	-0.70 ± 0.01	-0.10 ± 0.02
$\chi_{\perp,\max}$		1.80 ± 0.02	2.28 ± 0.02		-0.86 ± 0.05	
$\chi_\perp\ (T = 0)$		1.84 ± 0.02	2.41 ± 0.02			
EPR		2.025 ± 0.005	2.495 ± 0.005	2.72 ± 0.01		

the G_yA_x configuration (which implies $J_{\parallel}>0$).

For the Ga compound, the value of the exchange interaction parameter $J_{\perp}/k$, ranging between -0.70 K and -0.86 K, depending on the method employed in its determination, is in good accordance with the value -0.825 found for the Nd-Nd interaction in $NdFeO_3$. This result is quite reasonable since the average Nd-Nd distance in $NdGaO_3$ (3.87 Å) is quite similar to that in $NdFeO_3$ (3.902 Å).

In the present work we find that g_z is larger than the other two components in consistence with the Ising character of the statistical model that fits all the available thermodynamic data. This result is certainly in contradiction with our previous conjecture that an XY model anisotropy could be expected, but also from the rather isotropic values ($g_x=2.227$, $g_y=2.483$, and $g_z=2.549$) derived from inelastic neutron scattering.[4]

The origin of the previous misinterpretation of the heat capacity in terms of the $S=\frac{1}{2}$, s.c. XY model arose from our overconfidence in the excellent correspondence of the experimental critical energy and entropy to the model predictions. It becomes evident after the present work that similar critical energy and entropy contents may arise from Ising crossover models that are intermediate to the two extremes of the s.q. and s.c. model. (Table III). One may conclude that just from heat capacity measurements it is difficult to draw unambiguous conclusions as to the character of a magnetic phase transition, and it becomes evident now that single-crystal magnetic susceptibility data may yield enough information as to determine the applicability of a statistical model.

TABLE III. Comparison of theoretical predictions of the critical thermodynamical functions with the experimental values. (q = nearest-neighbor number).

	q	$kT_c/J_{\perp}$	S_c/R	$-E_c/T_c$
Ising s.q.	4	1.1346	0.30647	0.62323
Ising $\lvert r\rvert=0.1$	6	1.3807	0.48	0.36
Ising s.c.	6	2.2553	0.5579	0.2200
XY s.c.	6	2.0173	0.4628	0.45
H s.c.	6	1.68	0.43	0.60
$NdGaO_3$			0.46 ± 0.01	0.41 ± 0.04

ACKNOWLEDGMENTS

This work has been financed by the CICYT MAT96/0448 project.

[1] J. M. Phillips, J. Appl. Phys. **79**, 1829 (1996).

[2] S. Geller, Acta Crystallogr. **10**, 243 (1957).

[3] F. Bartolomé, M. D. Kuz'min, R. I. Merino, and J. Bartolomé, IEEE Trans. Magn. **30**, 960 (1994).

[4] W. Marti, M. Medarde, S. Rosenkranz, P. Fischer, A. Furrer, and C. Klemenz, Phys. Rev. B **52**, 4275 (1995).

[5] E. F. Bertaut, in *Magnetism*, edited by G. T. Rado and H. Suhl (Academic, New York, 1963), Vol. III.

[6] A. Podlesnyak, S. Rosenkranz, F. Fauth, W. Marti, A. Furrer, A. Mirmelstein, and H. J. Scheel, J. Phys.: Condens. Matter **5**, 8973 (1993).

[7] A. van der Bilt, K. O. Joung, R. Carlin, and L. J. de Jongh, Phys. Rev. B **22**, 1259 (1980).

[8] J. Bartolomé, E. Palacios, M. D. Kuz'min, F. Bartolomé, I. Sosnowska, R. Przenioslo, R. Sonntag, and M. M. Lukina, Phys. Rev. B **55**, 11 432 (1997).

[9] K. P. Belov, A. K. Zvezdin, A. M. Kadomtseva, and I. B. Krynetskii, Zh. Éksp. Teor. Fiz. **67**, 1974-83 (1974) [Sov. Phys. JETP **40**, 980 (1974)].

[10] A. Abragam and B. Bleaney, *EPR of Transition Ions* (Clarendon, New York, 1970), p. 854.

[11] R. Navarro and L. J. de Jongh, Physica B & C **94**, 67 (1978).

[12] F. Harbus and H. E. Stanley, Phys. Rev. **7**, 365 (1973).

[13] M. F. Sykes and M. Fisher, Physica (Amsterdam) **28**, 919 (1962).

[14] M. Fisher, J. Math. Phys. **4**, 124 (1963).

[15] L. Onsager, Phys. Rev. **65**, 117 (1944).

[16] T. Shinoda, H. Chihara, and S. Seki, J. Phys. Soc. Jpn. **19**, 1637 (1964).

[17] V. M. Orera, L. E. Trinkler, R. I. Merino, and A. Larrea, J. Phys.: Condens. Matter **7**, 657 (1995).

[18] I. Plaza, E. Palacios, J. Bartolomé, S. Rosenkranz, C. Ritter, and A. Furrer, Physica B **234-236**, 632 (1997).